J|A|C|S
ARTICLES
Published on Web 09/27/2007

Orientational and Dynamical Heterogeneity of Rhodamine 6G Terminally Attached to a DNA Helix Revealed by NMR and Single-Molecule Fluorescence Spectroscopy

Heike Neubauer, Natalia Gaiko,[†] Sylvia Berger,[‡] Jörg Schaffer,[§] Christian Eggeling, Jennifer Tuma, Laurent Verdier, Claus A. M. Seidel,*[,||] Christian Griesinger,* and Andreas Volkmer*[,⊥]

Contribution from the Max-Planck-Institut für Biophysikalische Chemie, Am Fassberg 11, 37077 Göttingen, Germany

Received March 31, 2007; E-mail: a.volkmer@physik.uni-stuttgart.de; cigr@nmr.mpibpc.mpg.de; cseidel@gwdg.de

Abstract: The comparison of Förster resonance energy transfer (FRET) efficiencies between two fluorophores covalently attached to a single protein or DNA molecule is an elegant approach for deducing information about their structural and dynamical heterogeneity. For a more detailed structural interpretation of single-molecule FRET assays, information about the positions as well as the dynamics of the dye labels attached to the biomolecule is important. In this work, Rhodamine 6G (2-[3′-(ethylamino)-6′-(ethylimino)-2′,7′-dimethyl-6′*H*-xanthen-9′-yl]-benzoic acid) bound to the 5′-end of a 20 base pair long DNA duplex is investigated by both single-molecule multiparameter fluorescence detection (MFD) experiments and NMR spectroscopy. Rhodamine 6G is commonly employed in nucleic acid research as a FRET dye. MFD experiments directly reveal the equilibrium of the dye bound to DNA between three heterogeneous environments, which are characterized by distinct fluorescence lifetime and intensity distributions as a result of different guanine−dye excited-state electron transfer interactions. Sub-ensemble fluorescence autocorrelation analysis shows the highly dynamic character of the dye−DNA interactions ranging from nano- to milliseconds and species-specific triplet relaxation times. Two-dimensional NMR spectroscopy corroborates this information by the determination of the detailed geometric structures of the dye−nucleobase complex and their assignment to each population observed in the single-molecule fluorescence experiments. From both methods, a consistent and detailed molecular description of the structural and dynamical heterogeneity is obtained.

Introduction

The determination of Förster resonance energy transfer (FRET) efficiencies between known positions of two fluorophores bound to biological macromolecules is a highly sensitive optical tool for estimating intramolecular distances in the range from 10 to 100 Å, which is inaccessible to other solution methods.[1−3] FRET has been widely used as a structural tool for nucleic acids as well as for the study of their interactions with small organic molecules and proteins under physiologically relevant solution conditions.[4−11] In recent years, an increasing number of single-molecule FRET studies have been reported that allow for monitoring the conformational dynamics of DNA and RNA structures in real time.[12−17] Most FRET assays employed in nucleic acid research take advantage of the high sensitivity, the selectivity, and the advancement of synthesis and conjugation chemistry of highly fluorescent donor and acceptor dyes, such as rhodamine, cyanine, and fluorescein dyes covalently attached to the end of an oligonucleotide using flexible alkyl linkers. The lack of information about the exact

[†] Present address: Procter & Gamble Services GmbH, Sulzbacherstr. 40, 65823 Schwalbach am Taunus, Germany.
[‡] Present address: Fluka Chemie GmbH, Industriestrasse 25, CH-9471 Buchs SG, Switzerland.
[§] Present address: Carl Zeiss, MicroImaging GmbH, Königsallee 9-12, 37081 Göttingen, Germany.
[||] Present address: Heinrich-Heine-Universität Düsseldorf, Lehrstuhl für Molekulare Physikalische Chemie, Universitätsstr. 1, 40225 Düsseldorf, Germany.
[⊥] Present address: Universität Stuttgart, 3. Physikalisches Institut, Pfaffenwaldring 57, 70550 Stuttgart, Germany.

(1) Stryer, L.; Haugland, R. P. *Proc. Natl. Acad. Sci. U.S.A.* **1967**, *58*, 719−726.
(2) van der Meer, B. W.; Cooker, G.; Chen, S. Y. *Resonance Energy Transfer: Theory and Data*; VCH Publishers: New York, 1994.
(3) Jares-Erijman, E. A.; Jovin, T. M. *Nat. Biotechnol.* **2003**, *21*, 1387.
(4) Steiner, R. F., Kuboto, Y. In *Excited States of Biopolymers*; Steiner, R. F., Ed.; Plenum Press: New York, 1983; pp 203−249.
(5) Clegg, R. M. *Methods Enzymol.* **1992**, *211*, 353−388.
(6) Clegg, R. M.; Murchie, A. I. H.; Zechel, A.; Lilley, D. M. J. *Proc. Natl. Acad. Sci. U.S.A.* **1993**, *90*, 2994−2998.
(7) Gohlke, C.; Murchie, A. I. H.; Lilley, D. M. J.; Clegg, R. M. *Proc. Natl. Acad. Sci. U.S.A.* **1994**, *91*, 11660−11664.
(8) Jares-Erijman, E. A.; Jovin, T. M. *J. Mol. Biol.* **1996**, *257*, 597−617.
(9) Vamosi, G.; Clegg, R. M. *Biochemistry* **1998**, *37*, 14300−14316.
(10) Lilley, D. M. J.; Wilson, T. J. *Curr. Opin. Chem. Biol.* **2000**, *4*, 507−517.
(11) Parkhurst, L. J. *Methods Enzymol.* **2004**, *379*, 235−262.
(12) Deniz, A. A.; Dahan, M.; Grunwell, J. R.; Ha, T.; Faulhaber, A. E.; Chemla, D. S.; Weiss, S.; Schultz, P. G. *Proc. Natl. Acad. Sci. U.S.A.* **1999**, *96*, 3670−3675.
(13) McKinney, S. A.; Declais, A.-C.; Lilley, D. M. J.; Ha, T. *Nat. Struct. Biol.* **2003**, *10*, 93−97.
(14) Li, H.; Ren, X.; Ying, L.; Balasubramanian, S.; Klenerman, D. *Proc. Natl. Acad. Sci. U.S.A.* **2004**, *101*, 14425−14430.
(15) Rasnik, I.; McKinney, S. A.; Ha, T. *Acc. Chem. Res.* **2005**, *38*, 542−548.
(16) Hodak, J. H.; Downey, C. D.; Fiore, J. L.; Pardi, A.; Nesbitt, D. J. *Proc. Natl. Acad. Sci. U.S.A.* **2005**, *102*, 10505−10510.
(17) Zhuang, X. *Annu. Rev. Biophys. Biomol. Struct.* **2005**, *34*, 399−414.

10.1021/ja0722574 CCC: $37.00

orientations and dynamics of the transition dipole moments of the fluorophores has prevented the use of intramolecular fluorophore distances derived from FRET efficiencies as exact restraints for a more detailed and quantitative interpretation of DNA structures. It is therefore expedient to acquire more knowledge about the exact structural dynamics of FRET moieties attached to the biopolymer of interest.

Previous efforts toward the determination of the exact position of a fluorophore tethered to the 5′-end of a double-stranded deoxyribonucleic acid (dsDNA), which represents a moiety of an FRET assay commonly employed in nucleic acid research, include the use of fluorescence depolarization spectroscopy,[18−21] nuclear magnetic resonance (NMR) spectroscopy,[21] and *ab initio* calculations.[22] When rhodamine and cyanine dyes were terminally attached to the DNA helix, the dye was found to interact with nucleotides.[19,21] For the dye Cy3, a single static structure where the fluorophore is stacked onto the end of the helix in a manner similar to that of an additional base pair was found despite the fact that the structure is quite dynamic,[21] e.g., judged from the lack of imino resonances at the terminal base pair. However, the above-mentioned studies on an ensemble of molecules usually fail to resolve distinct conformational states of the dye−DNA complexes and their exchange kinetics, which would require their synchronization. In contrast, evidence for the coexistence of more than one conformer of the dye−dsDNA complex was found by single-molecule fluorescence spectroscopy, capable of monitoring conformational changes in real time without the need for synchronization.[23−25] Prior to the work, which we will present here, it was not possible to assign a detailed geometric structure to the various conformational states of the dye-dsDNA complexes identified in single-molecule fluorescence studies.

We report the study of the structural dynamics of Rhodamine 6G (Rh6G, 2-[3′-(ethylamino)-6′-(ethylimino)-2′,7′-dimethyl-6′*H*-xanthen-9′-yl]-benzoic acid) coupled via a C6-linker to the nucleotide C21 at the 5′-end of a 20 base pair DNA duplex (Rh6G-dsDNA, Figure 1). Not only could we identify at least three conformers of the dye-labeled DNA complex by single-molecule fluorescence spectroscopy, but we were also able to determine the high-resolution structures of these conformers by two-dimensional NMR spectroscopy in conjunction with structure calculations. The NMR structures reveal two predominant conformers, in which the dye stacks over the terminal base pair of the dsDNA in two distinct orientations. A third conformation is found in which the dye does not show nuclear Overhauser effects (NOEs) to the DNA indicating that it is more or less free in solution. Evidence for the dynamic character of these conformations is provided by a fluorescence intensity autocorrelation as well as an NMR line width analysis. The implications

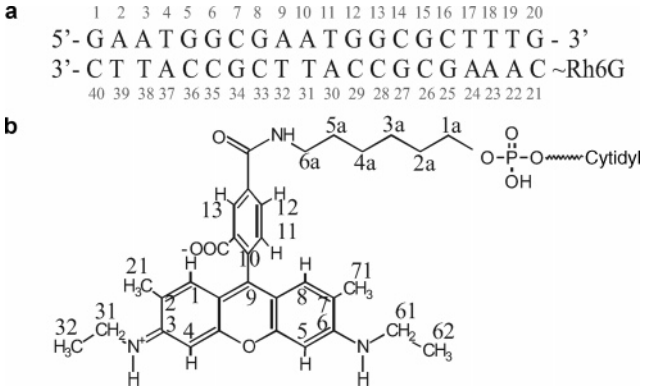

Figure 1. Sequence and the numbering scheme of the 20 base pair double-stranded DNA (a) and the aminoalkyl coupled Rhodamine 6G (b). The coupling of the dye via a hexamethyleneamine (C6) linker is to the 5′ phosphate group of the 5′-terminal C21.

of our results for the detailed structural interpretation of FRET efficiencies in nucleic acid research are discussed.

Materials and Methods

Rhodamine 6G Labeled DNA Preparation. For NMR experiments, the Rhodamine 6G-labeled oligomer Rh6G-d(5′-CAA AGC GCC ATT CGC CAT TC-3′) and its complementary strand d(5′-GAA TGG CGA ATG GCG CTT TG-3′) were purchased from BioSpring (Frankfurt/Main, Germany). The Rh6G-dsDNA duplex was formed from a mixture of both component strands with a molar ratio of 1:1 by annealing at 80 °C for 10 min in buffer containing 100 mM Na_2HPO_4/NaH_2PO_4 (pH 7.0, uncorrected for deuterium isotope effect) and allowing it to cool slowly to room temperature. Afterward, the duplexes were desalted with a PD-10 column (Amersham Pharmacia). Similarly, the unlabeled reference dsDNA was obtained from the unlabeled single strands.

For single-molecule experiments, Rhodamine 6G (Molecular Probes, Oregon) was covalently attached to the 5′-end of the oligonucleotide sequence d(5′-CAA AGC GCC ATT CGC CAT TC-3′), and the Rh6G-dsDNA duplex was assembled in a mixture of the dye labeled strand and its complementary unlabeled strand with a molar ratio of 1:5. The mixture was annealed by heating to 90 °C for 5 min in a buffer containing 360 mM NaCl, 24 mM sodium citrate, and 50 μM $MgCl_2$ (pH 7.0) and allowing it to cool slowly to room temperature. Similarly, the reference Rh6G-ds-T-DNA was obtained by labeling the oligonucleotide d(5′-**T** CAA AGC GCC ATT CGC CAT TC-3′) with Rhodamine 6G and hybridization with its complementary unlabeled sequence. All oligonucleotides and counterstrands were purchased from NAPS (Göttingen, Germany).

NMR Spectroscopy. NMR experiments were performed at 800 MHz on a DRX800 spectrometer (Bruker). ^{1}H nuclear Overhauser enhancement and exchange spectroscopy (NOESY) spectra with mixing times of 100, 150, and 200 ms, and double quantum filtered correlation spectroscopy (DQF-COSY) spectra were recorded in D_2O with a relaxation delay of 2.0 s, 48 scans per t_1 value, a spectral width of 7.8 ppm, 512 × 4096 (t_1,t_2) data points, apodized with a squared cosine function, and zero-filled to yield 2k × 8k (ω_1, ω_2). There was no need to suppress the zero-quantum cross-peaks in the NOESY spectra due to sufficiently short T_2 relaxation times of the protons. The spectra were processed on an Origin200 Silicon Graphics workstation using the program XWINNMR (Bruker, Karlsruhe, version 3.1). An automated baseline correction was applied in both dimensions. In order to check the integrity of the duplexes, 1D imino spectra were acquired in a mixture of 90% H_2O and 10% D_2O with a jump and return echo pulse sequence[26] applying a spectral width of 22 ppm and 16k points for the acquisition. ^{1}H NOESY spectra were assigned and integrated using FELIX 2000.1 (Biosym/MSI, San Diego). DQF-COSY spectra

(18) Clegg, R. M.; Murchie, A. I. H.; Zechel, A.; Carlberg, C.; Diekmann, S.; Lilley, D. M. J. *Biochemistry* **1992**, *31*, 4846−4856.
(19) Vamosi, G.; Gohlke, C.; Clegg, R. M. *Biophys. J.* **1996**, *71*, 972−994.
(20) Lorenz, M.; Hillisch, A.; Payet, D.; Buttinelli, M.; Travers, A.; Diekmann, S. *Biochemistry* **1999**, *38*, 12150−12158.
(21) Norman, D. G.; Grainger, R. J.; Uhrin, D.; Lilley, D. M. J. *Biochemistry* **2000**, *39*, 6317−6324.
(22) Hillisch, A.; Lorenz, M.; Diekmann, S. *Curr. Opin. Struct. Biol.* **2001**, *11*, 201−207.
(23) Edman, L.; Rigler, R. *Proc. Natl. Acad. Sci. U.S.A.* **1996**, *93*, 6710−6715.
(24) Wennmalm, S.; Edman, L.; Rigler, R. *Proc. Natl. Acad. Sci. U.S.A.* **1997**, *94*, 10641−10646.
(25) Eggeling, C.; Fries, J. R.; Brand, L.; Günther, R.; Seidel, C. A. M. *Proc. Natl. Acad. Sci. U.S.A.* **1998**, *95*, 1556−1561.
(26) Sklenar, V.; Bax, A. *J. Magn. Reson.* **1987**, *74*, 469−479.

were recorded for the assignment of the sugar protons and the H5, H6 cytosine aromatic protons of the dye-labeled and the reference dsDNAs. All spectra were obtained at 274 and 300 K in a buffer containing 100 mM NaCl and 20 mM Na_2HPO_4/NaH_2PO_4 (pH 7.0), and all chemical shifts were referenced to the signal for residual HDO in the 2D NOESY spectrum at 4.76 ppm at 300 K. Unless otherwise specified, the concentration of the Rh6G-dsDNA sample was 3 mM. For the experiments carried out in D_2O the dsDNA was lyophilized and dissolved in 300 μL of 99.999% D_2O purchased from Deutero.

NMR Structure Calculations. The peaks in the NOESY spectrum recorded at 150 ms were integrated, and the interproton distances were calculated based on the known distances for the cross-peak integrals of the aromatic protons of the dye. They were allowed to vary by $\pm$0.5 Å. All structure calculations were performed using the CNS_SOLVE 1.1 program. The starting right-handed structure (B-form) of the 20mer dsDNA labeled with Rhodamine 6G via an ϵ-aminohexyl-linker was built using INSIGHT II 2000.1 (Accelrys, San Diego). The force field of the B-form dsDNA was taken from the standard RNA-DNA-ALLATOM parameter file for nucleic acids. The parameters used for the dye and the linker were derived from the standard DISCOVER 3.0/INSIGHT II CVFF force field. The starting conformation was subjected to a simulated annealing protocol: 15 ps at 2000 K, then cooling for 15 ps to 0 K in steps of 50 K, and finally three cycles of 500 conjugate gradient minimization steps. Due to the observation of incompatible NOEs, two structures were calculated by assigning each experimental dye/DNA NOE to either one of the two or to both conformations, which are denoted as **A** and **B** (see Supporting Information Table 7). Thus, a total of 250 NOE-derived distance restraints (234 intra dsDNA, 12 inter dye-dsDNA, 4 intra dye) and a total of 243 NOE-derived distance restraints (234 intra dsDNA, 5 inter dye-dsDNA, 4 intra dye) were used for the calculation of the **A** and **B** conformation, respectively. Soft-square potentials with force constants of 200/200/100 kcal·mol^{-1}·Å^{-2} were applied. The hydrogen bonds were deduced from the imino/amino region of the NOESY spectra and introduced as distance constraints (51 hydrogen bonds) in the calculations. Additional planarity restraints using a force constant of 600 kcal·mol^{-1}·Å^{-2} were included for those nucleobases, which showed no chemical shift deviations from a canonical B-form dsDNA. All calculations were performed twice using both sets of NOEs yielding 100 structures each.

Fluorescence Spectroscopy. Single-molecule and resulting sub-ensemble data were obtained using a confocal microscope with linearly polarized laser excitation at 528 nm (180-ps pulses at a repetition rate of 73 MHz, average excitation intensity of 84 kW·cm^{-2}) and polarization-sensitive, dual-channel multiparameter fluorescence detection (MFD) using a PC-MFD-card (SPC 431, Becker&Hickl GmbH (Berlin, Germany)).[27,28] For ensemble fluorescence correlation spectroscopy (FCS) experiments, we used a hardware correlator (ALV-5000/E, ALV GmbH (Langen, Germany)) to record the cross-correlation of fluorescence intensity time traces monitored by the two detection channels. All measurements were made on freely diffusing molecules in buffer containing 10 mM Na_2HPO_4/NaH_2PO_4 and 180 mM NaCl (pH = 7.5) at room temperature. The final sample concentrations were $<10^{-12}$ M and $\sim10^{-9}$ M for single-molecule MFD and FCS experiments, respectively. Unless otherwise specified, the radial and axial 1/*e* radii of the Gaussian-approximated focal volume were 0.55 μm and 1.65 μm, respectively. Fluorescence quantum yields were determined from integrated ensemble emission spectra recorded on a Spex Fluorolog III (Instruments SA, Edison, New Jersey). The methods used for single-molecule data analysis and species-selective sub-ensemble spectroscopy are described in the Supporting Information.

Results

Conformational Heterogeneity Revealed by Single-Molecule MFD Burst Analysis. The fluorescence quantum yield of Rhodamine 6G is strongly reduced from 0.95 for the free dye to 0.15 for Rh6G-dsDNA, which is caused by proton-coupled electron transfer between the dye and the neighboring nucleobase guanine (G20) acting as the electron acceptor and donor,[29] respectively. By exploiting this efficient fluorescence quenching, we can determine the location of the dye relative to the DNA duplex. Using single-molecule MFD,[27,28,30] for each single Rh6G-dsDNA complex that diffuses through the open detection volume and is recognized by a fluorescence burst we observed marked differences in the time evolution of its fluorescence lifetime ($_F\tau$) without significant changes in the fluctuations of its fluorescence anisotropy ($_Fr$) and intensity (F). By constructing a cumulative weighted two-dimensional probability histogram of joint parameter values ($_F\tau$,$_Fr$) from more than a thousand individual Rh6G-dsDNA (Figure 2a), we resolve two clearly separated distributions: While the short fluorescence lifetime distribution with a mean of 1.3 ns indicates strong fluorescence quenching of the dye in a conformation that efficiently interacts with the guanine, the long lifetime distribution with a mean of 4.1 ns suggests a conformation, in which the dye shows less favorable and/or no electronic interaction with the guanine. This observation implies the existence of at least two main conformations of Rh6G-dsDNA, which we denote **A** and **B**/**C**, which can be distinguished via the excited-state lifetime of the dye and are stable within the dwell time inside the detection volume, i.e., within a few milliseconds.

The assignment of the long lifetime distribution to two conformations, **B** and **C**, stems from an MFD burst analysis with constant photon numbers that allows the direct comparison of standard deviations, σ, of measured fluorescence parameter distributions (for details, see Supporting Information). Unlike the unimodal lifetime distribution with $_F\bar{\tau} = 4.0$ ns and $\sigma = 0.55$ ns recorded for the free dye (cp. gray $_F\tau$-histogram in Figure 2a), the long fluorescence lifetime distribution ($_F\tau > 2.5$ ns) recorded for Rh6G-dsDNA is significantly broadened with $\sigma \approx 1.1$ ns, and its mean lifetime is shifted to slightly higher values, $_F\bar{\tau} = 4.1$ ns.[31] Both observations provide evidence for the existence of at least two conformational substates of Rh6G-dsDNA that account for the heterogeneous long lifetime distribution: For one conformer, denoted **B**, a reduced brightness and a fluorescence lifetime in excess of the radiative lifetime of the noninteracting chromophore are indicative of an electronic interaction of the dye with nucleobases without being quenched.[32,33] For the other conformer, denoted **C**, the fluorescence lifetime is not changed with respect to that of the free dye, which indicates the absence of a strong interaction of the dye with the dsDNA. More features of the states **A**, **B**, and **C** are discussed in the section Species-Selective MFD Spectroscopy below.

A state-specific burst-size distribution (BSD) fractions analy-

(27) Schaffer, J.; Volkmer, A.; Eggeling, C.; Subramaniam, V.; Striker, G.; Seidel, C. A. M. *J. Phys. Chem. A* **1999**, *103*, 331−336.
(28) Eggeling, C.; Berger, S.; Brand, L.; Fries, J. R.; Schaffer, J.; Volkmer, A.; Seidel, C. A. M. *J. Biotechnol.* **2001**, *86*, 163−180.
(29) Seidel, C. A. M.; Schulz, A.; Sauer, M. H. M. *J. Phys. Chem.* **1996**, *100*, 5541−5553.
(30) Widengren, J.; Kudryavtsev, V.; Antonik, M.; Berger, S.; Gerken, M.; Seidel, C. A. M. *Anal. Chem.* **2006**, *78*, 2039−2050.
(31) Zander, C.; Sauer, M.; Drexhage, K. H.; Ko, D. S.; Schulz, A.; Wolfrum, J.; Brand, L.; Eggeling, C.; Seidel, C. A. M. *Appl. Phys. B* **1996**, *63*, 517−523.
(32) Bixon, M.; Jortner, J.; Verhoeven, J. W. *J. Am. Chem. Soc.* **1994**, *116*, 7349−7355.
(33) Nord, S.; Sauer, M.; Arden-Jacob, J.; Drexhage, K. H.; Lieberwirth, U.; Seeger, S.; Wolfrum, J. *J. Fluoresc.* **1997**, *7*, 79S-81S.

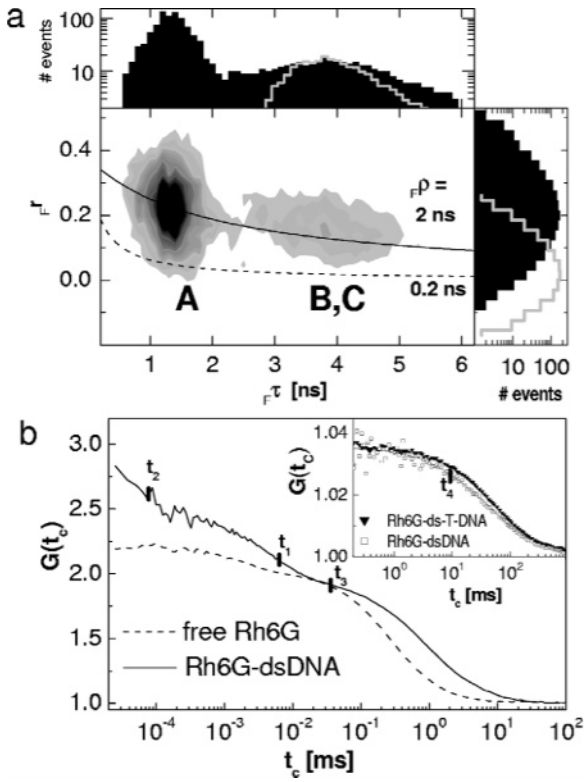

Figure 2. Conformational heterogeneity and dynamics revealed by single-molecule MFD and FCS spectroscopy. (a) Two-dimensional probability histogram of joint single-molecule fluorescence lifetime and steady-state anisotropy values ($_F\tau$,$_F r$) constructed from 1358 Rh6G-dsDNA molecules using a sliding window of 150 events. The frequency is increasing from bright to dark in a linear grayscale look-up table. The analysis of the single-parameter histogram projections (shown in log scale) yields a bimodal lifetime distribution with $_F\bar{\tau}_A = 1.3$ ns (standard deviation: $\sigma = 0.3$ ns) and $_F\bar{\tau}_{B,C} = 4.1$ ns ($\sigma \approx 1.1$ ns), and a common single anisotropy distribution with $_F\bar{r} = 0.20$ ($\sigma = 0.11$). For comparison, normalized single-parameter probability distributions with $_F\bar{\tau} = 4.0$ ns ($\sigma = 0.65$ ns) and $_F\bar{r} = 0.02$ ($\sigma = 0.08$ ns) are observed for the free Rhodamine 6G (shown in gray). The mobility of the bound and free dye is best described by a mean rotational correlation time ($_F\bar{\rho}$) of 2 and 0.2 ns (overlaid solid and dashed lines), respectively. (b) FCS curves for the Rh6G-dsDNA (solid line) in comparison to the free Rhodamine 6G sample (dashed line), as measured in a detection volume defined by a radial (axial) radius of 0.55 μm (1.65 μm). Insert: FCS measurements with an expanded detection volume defined by a radial (axial) radius of 3.7 μm (25 μm) for Rh6G-dsDNA (□) compared to Rh6G-ds-T-DNA (▼). See text for fit results.

sis[34] with a threshold for the discrimination of the short and long fluorescence lifetime distributions set to 2.5 ns (for details, see Supporting Information) reveals an 82:18 population ratio (or an equilibrium reaction constant of K_{eq}(BSD) = 0.22) between the conformations **A** and **B/C**.

The mobility of the dye in the two predominant conformations (**A** and **B**) is best described by a common mean rotational correlation time of $_F\bar{\rho} = 2$ ns, calculated from the Perrin equation, $_F\bar{\rho} = {}_F\bar{\tau}\,{}_F\bar{r}/({}_F r_0 - {}_F\bar{r})$, and a fundamental anisotropy for Rhodamine 6G of $_F r_0 = 0.375$.[35] This indicates a significantly restricted rotational motion of the chromophore when interacting with the dsDNA. In comparison, for the free Rhodamine 6G in solution, we obtained a unimodal distribution of the steady-state anisotropy about its mean value $_F\bar{r} = 0.02$, which is expected for a homogeneous sample consisting of a single fluorescent species (gray parameter distribution in Figure 2a). The fast rotational motion of the free dye is best described by a mean rotational correlation time of $_F\bar{\rho} \approx 0.2$ ns. The observed lack of strong interaction of the dye with the dsDNA in conformer **C** may suggest a high mobility of the dye in this conformation, which may approach that of the free dye. However, within the statistical accuracy of our experiment with shot noised broadened distributions, it is not possible to find a separate distribution for species **C**. Thus, there is no direct evidence for a 0.02−0.05 component in the observed steady-state fluorescence anisotropy distribution ($_F\bar{r}$-histogram in Figure 2a) that can be distinguished from the two stacked conformers of predominant populations.

Conformer Dynamics Revealed by Fluorescence Correlation Spectroscopy (FCS). The preceding single-molecule fluorescence burst measurements reveal heterogeneity in the environments for the dye bound to dsDNA. To provide evidence for the dynamic character of the dye's interactions with dsDNA, we compared ensemble FCS experiments of Rh6G-dsDNA with that of the free dye (Figure 2b). Besides differences in the translational diffusion times due to different molecular sizes, the FCS curves show prominent differences at shorter correlation times. According to a standard FCS model (Supporting Information), the correlation curve analysis for the free dye results in a single-exponential decay term with a relaxation time $t_1 = 1.8$ μs that is attributed to the dye's triplet kinetics. In contrast, the curve for Rh6G-dsDNA exhibits three exponential decay components: The first decay component with $t_1 = 6.5$ μs is assigned to the dye's triplet kinetics because its correlation amplitude and time are dependent on the laser excitation intensity.[36] The second decay component with $t_2 = 80$ ns is attributed to the kinetics of complex formation between the dye and the nucleobases, which results in strong fluorescence quenching.[37] The third decay component with a correlation time of $t_3 = 10-100$ μs and an amplitude below 0.1 cannot accurately be determined because it cannot be clearly distinguished from the triplet term occurring on a similar time scale. However, both the correlation time and amplitude were found to be independent of laser excitation intensity, which indicates the existence of an additional ground state equilibrium reaction between two fluorescent states of distinct quantum efficiencies.

To determine quantitatively whether the interconversion between the conformations **A** and **B/C** occur on the millisecond time scale, we carried out FCS experiments with an expanded focal volume resulting in a prolonged observation time of the dye-labeled dsDNA. We compared the FCS curves for Rh6G-dsDNA with that recorded for a reference sample, Rh6G-ds-T-DNA, where we introduced an additional A−T base pair between the G20−C21 base pair and the dye resulting in a strongly reduced fluorescence quenching of the dye by guanine. Although both molecules are very similar in molecular size and, thus, have an identical translational diffusion time of about 47 ms, their correlation curves are markedly different in the millisecond time range (insert in Figure 2b). Only for Rh6G-dsDNA, where fluorescence quenching occurs, an additional decay term with a relaxation time of $t_4 = 9$ ms and an amplitude of 0.13 ± 0.02 is required to fit the data besides the previously identified decay terms occurring on faster time scales. Because

(34) Fries, J. R.; Brand, L.; Eggeling, C.; Köllner, M.; Seidel, C. A. M. *J. Phys. Chem. A* **1998**, *102*, 6601−6613.
(35) Kawski, A. *Crit. Rev. Anal. Chem.* **1993**, *23*, 459−529.
(36) Widengren, J.; Mets, Ü.; Rigler, R. *J. Phys. Chem.* **1995**, *99*, 13368−13379.
(37) Widengren, J.; Dapprich, J.; Rigler, R. *Chem. Phys.* **1997**, *216*, 417−426.

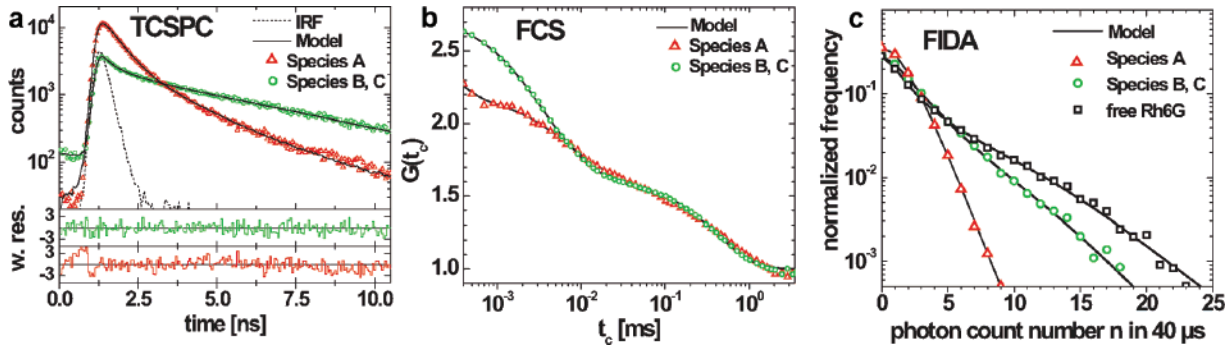

Figure 3. Sub-ensemble MFD spectroscopy of the two lifetime populations (**A**) (red triangle) and (**B**/**C**) (green circles). The model functions are shown as black lines. The error of the fitted parameter is estimated to be approximately 30%. (a) TCSPC (eq S10): The short fluorescence lifetime population **A** has at least three decay times with the corresponding species fractions: ${}_F\tau_1(x_1) = 3.1$ ns (9%), ${}_F\tau_2(x_2) = 0.9$ ns (32%), and ${}_F\tau_3(x_3) = 0.3$ ns (59%) with an additional contribution of scattered background light $B(t)$ of 18%. The long lifetime population **B**/**C** has at least two decay times with the corresponding species fractions: ${}_F\tau_1(x_1) = 4.5$ ns (64%) and ${}_F\tau_2(x_2) = 0.6$ ns (36%) with an additional contribution of scattered background light $B(t)$ of 10%. (b) FCS curves with the relaxation times t_i and the corresponding amplitudes c_i in brackets and the apparent average molecule number N (eq S11). The short lifetime population **A** has four relaxation terms with $N = 0.90$: Triplet $t_1 = 6$ μs (0.3), dye nucleobase complex formation $t_2 \leq 200$ ns (0.35), conformational dynamics $t_3 = 40$ μs (0.15), and transport term $t_4 = 0.50$ ms (0.3). The long-lifetime population **B**/**C** has three relaxation terms with $N = 0.65$: Triplet (species 1) $t_1 = 7$ μs (0.27), triplet (species 2) $t_2 = 2$ μs (0.26), and transport term $t_3 = 0.45$ ms (0.3). (c) FIDA histograms with a specific brightness Q_i and mean molecule number N_i as well as the fraction in brackets (eq S12). The FIDA histogram of the short lifetime population **A** is dominated by a single species with $Q(A) = 1$ (2.3; 98.7%) and Q(impurity) = 5.4 (0.03; 1.3%). The FIDA histogram of the long lifetime population **B**/**C** shows the existence of two species with Q(B) = 1.5 (1.0; 70%) and Q(C) = 5.3 (0.43; 30%). The histogram of Rh6G obtained under the same measurement conditions is shown for comparison (black squares).

of increased photobleaching of the dye in this experiment with prolonged dwell times, both the obtained decay time and amplitude are biased toward smaller values and should be regarded as lower bounds only. We attribute the additional millisecond decay component to a ground state equilibrium reaction between a dim and a bright fluorescent state, which are most probably accounted for by the observed short (conformer **A**) and long (conformers **B** and **C**) lifetime distributions, respectively. The fluorescence brightness ratio between the two distributions was determined to be about 0.238, which by using eq S8 given in the Supporting Information yields an FCS equilibrium constant of K_{eq}(FCS) ≈ 0.26. This value is in good agreement with K_{eq}(BSD) = 0.22 obtained independently from BSD analysis.

Using K_{eq}(BSD) $\cong 0.22$ together with the observed lower bound for the FCS decay time of 9 ms, we estimate the limits of absolute reaction rate constants for the population and depopulation of the conformational state **A** to ≤ 91 s^{-1} and ≤ 20 s^{-1}, respectively.

Species-Selective MFD Spectroscopy. Instead of analyzing the ensemble-averaged fluorescence properties given by the sum of all fluorescent species, species-selective MFD spectroscopy allows for the direct and unequivocal determination of fluorescence properties of its individual summands. In this way, specific details on the identified conformers **A**, **B**, and **C** are accessible. We performed sub-ensemble spectroscopy, which provides dynamics information on distinct time scales (*vide infra*), such as fluorescence decay analysis by time-correlated single-photon counting (TCSPC) (Figure 3a), fluorescence fluctuation analysis by FCS (Figure 3b), and brightness evaluation by fluorescence intensity distribution analysis (FIDA) (Figure 3c). Selective analysis of the short and long fluorescence lifetime populations of Figure 2a is achieved by separately averaging only bursts with ${}_F\tau < 2.5$ ns and ${}_F\tau > 3$ ns, respectively. The TCSPC histograms in Figure 3a directly reveal that the fluorescence decay curves of both lifetime populations are not single-exponential; i.e., the environment of the fluorophore is heterogeneous on time scales larger than several fluorescence lifetimes (approximately >10 ns). The decay curve of the short lifetime population **A** exhibits three decay components with lifetimes, ${}_F\tau_i$, and corresponding species fractions, x_i (eq S10), which is indicative of a dynamic system with at least three distinct species: ${}_F\tau_1(x_1) = 3.1$ ns (9%), ${}_F\tau_2(x_2) = 0.9$ ns (32%), and ${}_F\tau_3(x_3) = 0.3$ ns (59%). The long lifetime population of the states **B**/**C** reveals at least two decay components, ${}_F\tau_1(x_1) = 4.5$ ns (64%) and ${}_F\tau_2(x_2) = 0.6$ ns (36%), where ${}_F\tau_1$ is larger than the radiative lifetime of free Rh6G. This result directly confirms our conclusions obtained from our MFD burst analysis (Figure 2a). The conformational dynamics and the heterogeneity of **A** and **B**/**C** are also confirmed by species-selective correlation curves (Figure 3b). Besides the common diffusion term, three and two additional exponential decay terms are found for the short and long fluorescence lifetime populations, respectively (eq S11). The decays due to triplet population and depopulation are identified via their characteristic dependence on the irradiance. While a single triplet term with a relaxation time of 6 μs is found for the short lifetime population **A**, two triplet terms with relaxation times of 7 μs and 2 μs are found for the long lifetime population **B**/**C**. These results are consistent with the ensemble FCS data (Figure 2b) and independently confirm the presence of two conformers **B** and **C** due to their distinct triplet properties. Moreover, the correlation curve of conformer **A** exhibits two kinetic terms with relaxation times of approximately 40 μs and <200 ns. The latter relaxation time is limited by the dead time of the MFD acquisition board. We can unequivocally conclude that both the decay with $t_1 \approx 100$ ns, which is attributed to dye−nucleobase complex formation relaxation, and the relaxation process with $t_3 \approx 10-100$ μs found in ensemble FCS (Figure 2b) are exclusively ascribed to the dynamics of conformer **A**. FIDA complements this picture by providing information on the fluorescence brightness, Q, of the distinct species with a time resolution of 40 μs (Figure 3c). The FIDA histogram of the short lifetime population **A** is well described by a single species with a specific brightness of $Q(A) = 1$ (red triangles), which corresponds to 17% of the brightness of free Rh6G, Q(Rh6G) = 5.8 (black squares). In contrast, at least two

species with specific brightnesses, $Q(\mathbf{B}) = 1.5$ (70%) and $Q(\mathbf{C}) = 5.3$ (30%), are required to fit the FIDA histogram of the long lifetime population (green circles), which directly proves the existence of at least two species, **B** and **C**, respectively.

In summary, sub-ensemble fluorescence spectroscopy gives a consistent picture of the dynamics of all three species based on their distinct fluorescence and triplet properties. Depending on the time resolution of the different spectroscopic techniques employed (TCSPC: >10 ns, FCS: >125 ns (technical limit); FIDA: >40 μs, and MFD burst analysis: >1 ms), each technique resolves the dynamic heterogeneity of the three species at different time scales. Taking species **A** as an example, it displays fast fluorescent decays of at least three quenched species on time scales of nanoseconds as revealed by TCSPC analysis that are dynamically averaged when observed on time scales $\geq$40 μs. Thus, the FIDA and MFD burst analysis only detect a single apparent species with a single brightness. FCS independently confirms the results of both TCSPC and FIDA: As expected for the interconversion between the three species, two FCS relaxation times are found at $t_1 \approx 100$ ns and $t_3 \approx 10-100$ μs, which fall within the time range given by the time resolutions of both techniques. In comparison, the dynamic properties of the long lifetime population **B**/**C** are quite different: FIDA, FCS, and MFD burst analysis reveal that this population is static during the dwell time of the molecule. It consists of at least two species, where only one of them, species **B**, is strongly quenched. Taking this result into account, the interpretation of the TCSPC data is then as follows: The long lifetime component ${}_F\tau_1 = 4.5$ ns represents actually the sum of the fluorescence lifetime ${}_F\tau_1(\mathbf{C}) = 4$ ns and an additional long decay time ${}_F\tau_1(\mathbf{B}) > 4.5$ ns, which cannot be directly resolved in the time window of TCSPC. The low relative brightness of species **B** of 0.25 compared to the free dye indicates strong interactions with nucleobases. As for species **A**, TCSPC proves that species **B** is heterogeneous and consists of at least two species, i.e., a ground state complex with ${}_F\tau_1(\mathbf{B}) > 4.5$ ns possessing a very long radiative lifetime[33] and a quenched substate with ${}_F\tau_2(\mathbf{B}) = 0.6$ ns. See Supporting Information for further details on the species-selective MFD spectroscopy.

Fluorescence Control Experiments with Additional Oligonucleotide Sequences. To elucidate the questions which of the nearest-neighbor guanines in the sequence of Rh6G-dsDNA (G15, G25, or G20 in Figure 1a) influence the fluorescence quenching efficiency of the attached dye, and how this is affected by the dye's local geometries, we studied a set of additional oligonucleotide sequences for comparison. Based on such control experiments, which are summarized in supplemental Figures 6 and 7 and supplemental Table 2, we can conclude that the fluorescence properties of Rh6G-dsDNA are strongly dominated by the interaction with the adjacent terminal G20−C21 base pair and are influenced by geometric constraint factors, such as the linker length of the spacer and the dye orientation.

NMR Spectroscopy. We used nuclear Overhauser enhancement and exchange spectroscopy (NOESY)[38,39] and double quantum filtered correlation spectroscopy (DQF-COSY)[40,41] to assign proton resonances of the oligonucleotides and the Rhodamine 6G in the bound and the free form. Analysis was based on the NOE and chemical shift changes as well as the existence or absence of base−base hydrogen bridges according to the observation of the base imino protons. Almost complete assignment could be obtained. All spectra and observed chemical shift values are provided in supplemental Figures 8−11 and supplemental Tables 3−5:

The two-dimensional NOESY spectrum of the unlabeled reference dsDNA shows the typical Watson−Crick NOE connectivities between the imino and amino resonances except for the terminal G1-C40, A2-T39, T19-A22, and G20-C21 base pairs (Supporting Information Figure 8a). The missing connectivities are expected because of the fraying effect of terminal base pairs. In contrast, the NOESY spectrum of the Rh6G-dsDNA complex shows the peaks for the T19 and G20 imino protons (Supporting Information Figure 8b). This indicates that in the case of the dye-labeled dsDNA the fraying of the T19−A22 and G20−C21 base pairs is reduced, which suggests stacking of the dye with the terminal G20−C21 base pair. This is in contrast to the behavior of the dye Cy3, which did not stop the fast exchange of the imino proton of the terminal base pair with the water.[21]

The conformation of the dye behaves as expected (Supporting Information Figure 9): The free form shows a conformation in which the phenyl ring of the dye is perpendicular to the tricyclus rendering the two halves enantiotopic and thus chemically equivalent. For the dye attached to the dsDNA the enantiotopic halves of the dye become diastereotopic due to the chirality of the dsDNA, as can be appreciated from the protons RhH1, RhH4, RhH5, and RhH8.

Compared to the reference dsDNA, the H1′, H5, and H6 resonances of C21 are substantially shifted to higher fields, whereas the H8 resonance of G20 is shifted to lower fields (Supporting Information Figure 10).

In the aromatic part of the ^{1}H NOESY spectra of the Rh6G-dsDNA (Supporting Information Figure 11), we observed unambiguous NOE cross-peaks between the protons of the dye and the aromatic protons and H1′ protons of the terminal G20−C21 nucleotide pair exclusively. We do not observe NOEs with other bases thus no interaction of the dye to any other nucleotide than the terminal ones, which is in agreement with the result of the fluorescence studies.

In addition, we observed two NOE peaks in the NOESY spectrum of Rh6G-dsDNA, which belong to the ethyl or methyl group of the Rhodamine 6G. Because the ethyl or methyl resonances do not show any NOEs to other resonances, we attribute these NOE peaks to another conformational state, in which the attached dye does not interact with the dsDNA protons, such as the dye dangling in solution. From the peak intensities follows that the corresponding population is below 5%.

The NOESY spectrum also shows weak cross-peaks that indicate a dimerization of Rh6G-dsDNA via a stacking interaction of the dye. This process is inferred from the observation of long-range NOE peaks (NOESY and rotating frame Overhauser enhancement spectroscopy (ROESY)[42] performed) between protons that are too distant to show an intramolecular NOE, such as H4 and H11. The population of the dimer was

(38) Piotto, M.; Saudek, V.; Sklenar, V. *J. Biomol. NMR* **1992**, *2*, 661−666.
(39) Sklenar, V.; Piotto, M.; Leppik, R.; Saudek, V. *J. Magn. Reson. A* **1993**, *102*, 214−245.
(40) Aue, W. P.; Bartholdi, E.; Ernst, R. R. *J. Chem. Phys.* **1976**, *64*, 2229−2246.
(41) Kessler, H.; Gehrke, M.; Griesinger, C. *Angew. Chem., Int. Ed. Engl.* **1988**, *27*, 490−536.
(42) Bax, A.; Davis, D. G. *J. Magn. Reson.* **1985**, *63*, 207−213.

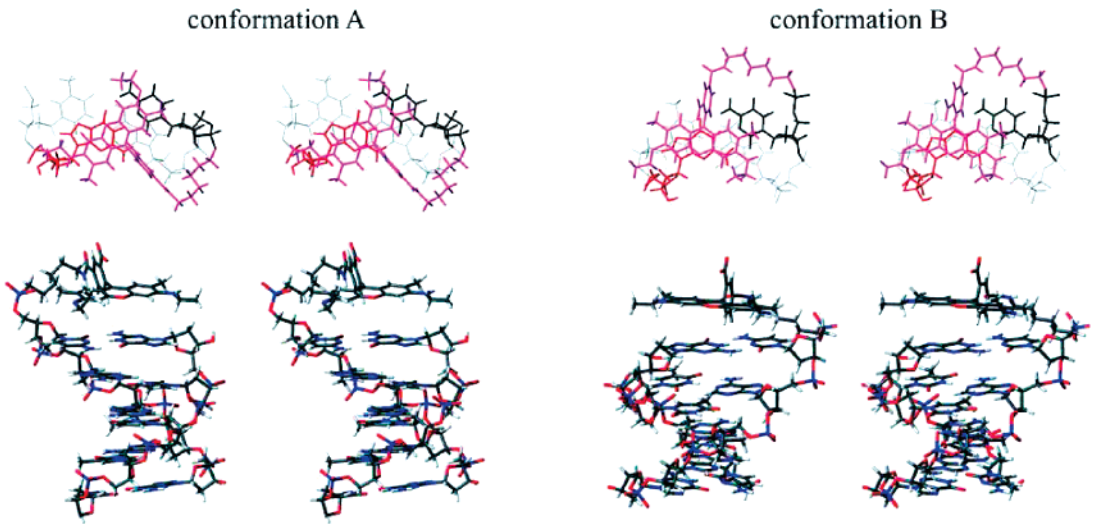

Figure 4. Stereo-representations from the top and side of the two calculated NMR structures for conformations **A** (80%) and **B** (20%) of the Rhodamine 6G-labeled dsDNA, which show the stacking of the dye onto the terminal G−C base pair.

found to be between 10% and 15% at 274 K and decreased with increasing temperature as expected. Dimer formation was corroborated by optical measurements on Rh6G in polar solvents at millimolar concentrations.

NMR Structure Calculations. A qualitative interpretation of the cross-peaks indicates that the conjugated tricyclic ring of the Rhodamine 6G stacks onto the G20−C21 base pair of the dsDNA. By running extensive restrained molecular dynamics calculations using all observed NOEs, however, we found that it is impossible to fulfill all NOEs with a single conformation of the Rh6G-dsDNA complex. Two NOEs, i.e., H12(Rh6G)/H5(C21) and H12(Rh6G)/H1′(C21), were consistently violated. Based on this finding, we performed calculations assuming two conformations that interconvert on a time scale faster than the differences of the chemical shifts involved. Using a procedure outlined in detail in the Materials and Methods section, we derived the structures for the two conformers where the dye stacks over the terminal G20−C21 base pair of the dsDNA (Figure 4):

While in the major conformation (denoted **A**) of Rh6G-dsDNA the phenyl ring of the dye is located over the minor groove of the dsDNA, it is located over the major groove in the minor conformation (denoted **B**). Furthermore, the linker extends the backbone of the dsDNA in the minor conformation **B**, whereas it extends in the opposite direction in the major conformation **A**. The dye is rotated by approximately 125° in the two conformations (Supporting Information Figure 12). In both conformations, we observed a distance of the tricyclic ring system of the Rhodamine 6G to the terminal G20−C21 base pair of 3.5 Å, which is in excellent agreement with an average value of 3.47 Å for the plane-to-plane distance between bases in B-type dsDNA. This observation is within the expectation that the structure of Rh6G-dsDNA is energetically minimized, namely by optimizing the stacking between the tricyclic ring and the G20−C21 base pair, which concurrently minimizes the contact of the hydrophobic base planes with water.

A population ratio between the two conformations of about 80:20 and their identity could be corroborated by comparison to a dsDNA labeled with tetramethylrhodamine (TMR) where the population ratio of the two conformations is approximately 1:1 (to be published). Taking the additional conformation denoted **C** with a population below 5% into account, in which the dye is not interacting with the dsDNA, renormalization yields lower bounds for the populations of conformation **A** and **B** of 76% and 19%, respectively. Due to the small population of the dimer of approximately 10% at NMR concentration, we do not expect a population change between **A** and **B** at concentrations used for NMR or single-molecule fluorescence experiments (vide infra).

Conformer Dynamics Revealed by NMR Line Width Analysis. The fluorescence experiments suggest a population and depopulation of the major conformation **A** with rates of $\leq$91 Hz and $\leq$20 Hz, respectively. However, no exchange process that would yield a corresponding line broadening of the major conformation by 20 Hz/π could be found neither for the resonances of the terminal G20−C21 base pair nor for the well separated Rhodamine 6G proton resonances RhH1, RhH4, RhH5, and RhH8 in the NOESY spectrum. For the line width analysis, we carefully measured all relaxation contributions to the line width yielding eq S1, as outlined in detail in the Supporting Information and supplemental Table 6. According to our calculations, the upper limits of the exchange rates for the selective dye protons of Rhodamine are in the range 12.3 to 16.5 Hz. Note that the chemical shift anisotropy is different for each of the dye protons and can also contribute differently to the line widths. This can explain their different exchange rates. As a result of the line width analysis, we can state that for the present NMR studies performed at millimolar concentrations there is no evidence for an exchange process with a rate faster than 16.5 Hz, which is slightly lower than the upper limit derived from the fluorescence measurements at nanomolar concentrations.

If there was a conformation that is populated and depopulated with rate constants of $\leq$91 Hz and $\leq$20 Hz, respectively, the NMR resonances should show a line broadening of 20/π Hz on top of the homogeneous line widths, assuming that the second conformation has chemical shift differences with respect to the major one of at least 20 Hz. Although this is an assumption, it is a well warranted one since any dislocation of the dye from the position it occupies in the major conformation would induce strong changes of the ring current effects on the chemical shifts of the G20−C21 base pair as well as on the resonances of the

Table 1. Interpretation of NMR and Single-Molecule Fluorescence Results and Assignment of the Individual Conformations, as Sketched in Figure 5

conformations/ methods	**A**	**B**	**C**
NMR	stacked conformation of dye over terminal G-C base pair (95 %)		conformation with dye distant from DNA (5 %)
(1) structure calculation	phenyl ring of dye is over minor groove (76 %)	dye rotated by ~125° and stacks more over G than C with phenyl ring over major groove (19 %)	--
Fluorescence	one state: efficient dye-guanine interaction	two states: less favorable dye-guanine interactions	
single-molecule: *(1) MFD* *(2) BSD analysis*	${}_F\bar{\tau} = 1.3$ ns (82 %)	${}_F\bar{\tau} = 4.1$ ns (18 %)	
sub-ensemble: *(3) FCS, TCSPC FIDA*	three species: dye-nucleobase complexes and quenched immobile dye ($Q = 1$)	less quenched immobile dye ($Q = 1.5$)	bright mobile dye ($Q = 5.3$)
	two relaxation times: < 200 ns and 50 μs for fast transitions between different fluorescing conformers (82%)	no relaxation times between 300 ns - 100 μs (13 %)	no relaxation times between 300 ns - 100 μs (5%)

dye itself. It is highly improbable that there is no resonance whose chemical shift is not changed by more than 20 Hz. We should stress that, on a similar system of TMR where the population of the two conformers is 1:1, we also do not observe two sets of signals, but rather one. The exchange rate as determined by MFD analysis is similar for this dye (data not shown).

A deceleration of the interconversion between the minor and major conformations with decreasing concentrations may account for the observed discrepancy between NMR and single-molecule observations. At the high concentrations necessary for NMR measurements, bimolecular interactions are favored that can disturb intramolecular interactions. To test this hypothesis, we have initially performed single-molecule fluorescence experiments where unlabeled dsDNA has been added up to millimolar concentrations, thus, mimicking the concentrations used in the NMR experiments. At such high concentrations, we found that fluorescent impurities in unlabeled dsDNA simply overwhelm the actual signal from a single Rh6G-dsDNA complex at more than 6 orders of magnitude lower concentrations. Because this fluorescence-based approach failed, a concentration-dependent NMR study has been carried out. Evidence for our supposition is provided from the concentration dependence of the imino resonance of G20. This resonance starts to split in two at low concentrations (below 500 μM) and appears as a single resonance at 1.4 mM, which was the concentration used for structure determination (see Supporting Information Figure 13). Despite the fact that the second imino G20 resonance has the same chemical shift as that of G20 imino in the unlabeled reference dsDNA, we can exclude that the second resonance stems from conformation **C**. This is because the population ratio between these two conformations was determined to be about 4:1, which is in striking agreement with the population ratio between conformations **A** and **B** obtained from structure calculations. It should be mentioned that the effect is much more pronounced for the mentioned TMR system which corroborates the assignment of the additional imino resonance.

For the additional set of signals of the dye that do not show NOEs to dsDNA, which is assigned to conformation **C**, the rate by which this state is generated from the state corresponding to the main set of signals must be smaller than 10 Hz according to the above results.

Discussions

Conformer Structures. Both NMR and single-molecule fluorescence measurements of the Rhodamine 6G bound to the 5′-end of a 20-base pair DNA duplex via an ϵ-aminohexyl-linker are summarized in Table 1 and reveal the following consistent picture (Figure 5): The dye tightly stacks onto the terminal base pair of the dsDNA to an extent that fraying of this terminal base pair is prevented. Otherwise, the structure of the dsDNA is only marginally influenced. At least three unequally populated conformations of the dye have been identified based on the heterogeneous single-molecule fluorescence lifetime distribution and triplet transition kinetics as well as on NOEs that are only compatible with at least two conformations in fast exchange and a third conformation that does not interact with the DNA. Remarkably, the population ratio between the two main conformations is consistently found to be approximately 4:1 in both studies. Therefore, we assign the short and long single-

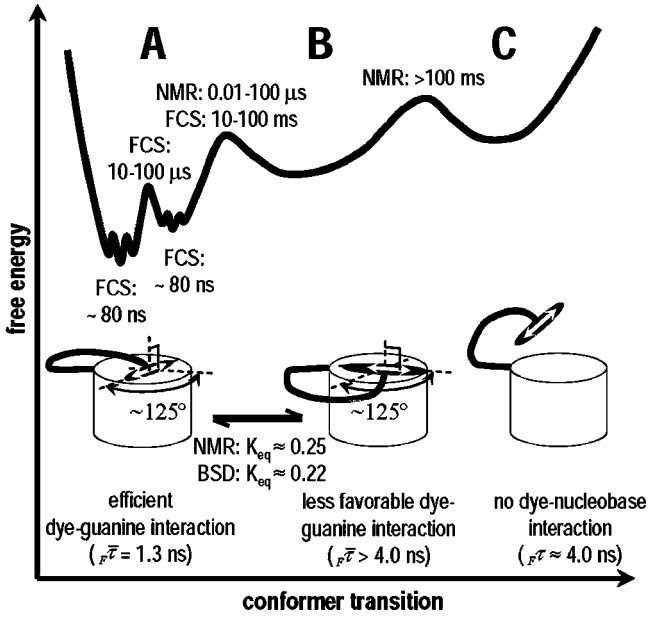

Figure 5. Proposed energy landscape summarizing the conformer transitions, their time scales of exchange, and schematic structures. The NMR structures of the two stacked conformations **A** and **B** differ in the orientation of the dye's transition moment over the terminal base pair and in its fluorescence quenching efficiency. An arbitrary structure of conformer **C** is shown, in which the dye was found to be distant from the nucleobases.

molecule fluorescence lifetime distribution to the NMR structures of conformation **A** and **B**, respectively (Figure 4). In conformation **A** of the major population, the dye stacks over the terminal G20−C21 base pair whereby the phenyl ring is pointing to the minor groove of the DNA helix. This conformer facilitates efficient quenching of the dye in close proximity to the guanine base G20 via excited-state electron transfer. The conformation of the minor population **B** is defined by an ~125° rotation of the dye over the G20−C21 base pair about the helix axis of the dsDNA with the phenyl ring pointing to the major groove. In this conformation, the dye stacks with a less favorable electronic interaction to guanine,[32,33] which results in a lifetime component that is longer than the radiative lifetime. The observed distance of the tricyclic ring system of the Rhodamine 6G to the terminal C−G base pair is 3.5 Å, which is in excellent agreement with an average value of 3.47 Å for the plane-to-plane distance between bases in B-type dsDNA. Moreover, a small population of a third conformation **C** (<5%) was consistently identified by both techniques, in which the dye is distant from the nucleobases and is essentially not quenched. At millimolar concentrations of the NMR measurements, a fourth species formed by dimerization of two DNA double strands via the dye is observed.

Transition Rates and Energy Landscape. We propose a unified energy landscape of the identified Rh6G-dsDNA conformer transitions and their respective time scales of exchange (Figure 5). Although the interconversion between conformer **A** and **B** is consistently described by an equilibrium constant of about ~0.25 by two independent experimental methods, both conformers are exchanging on strikingly different absolute time scales, i.e., between the rotational diffusion correlation times of 10 ns and 100 μs in NMR studies at millimolar concentrations and between 10 and 100 ms in fluorescence studies at pM concentrations. We found evidence that the reaction rates involved in this equilibrium reaction are concentration dependent. The most probable interpretation of this finding is that autocatalytic bimolecular collisions or the dimer that we could identify from NMR and fluorescence measurements facilitate the interconversion between the conformations **A** and **B**. Considering also the fact that a change of binding position from the minor (**A**) to major (**B**) groove involves the intermediate loss of the stacking interactions, a slow process in the millisecond time scale is likely to be expected for this transition due to the high activation barrier.

The time scale of the exchange between the stacked conformations, **A** and **B**, and the dye conformation, **C**, that is not interacting with the DNA exceeds 100 ms, as obtained from NMR line width analysis.

Fluorescence correlation experiments provide evidence for the dynamic character of the dye−dsDNA interactions on the nano- and microsecond time scale, which we attribute to kinetic processes where the dye−nucleobase stacking distance is fluctuating. Since these processes occur on a time scale faster than the millisecond lifetimes of the two main conformers and result in a modulation of the quenched fluorescence of the dye, we conclude that these fast ground state equilibrium reactions take place between substates within the major conformation **A** and **B**. Moreover sub-ensemble TCSPC and FCS indicate that at least three substates with distinct brightnesses exist in conformation **A**, which interconvert with characteristic relaxation times of 100 ns and 10−100 μs. This dynamics is too fast to be detected in the present series of NMR experiments; i.e., the structures given (Figure 4) represent structures with a mean position of the dye.

Implications for FRET. Next, we discuss important consequences of our results for an accurate determination of FRET distances in DNA structures. Briefly, we recall that the measured transfer efficiency exhibits a well-known dependence not only on the scalar distance separating a donor and an acceptor fluorophore covalently attached to the DNA helix but also on their fluorescence quantum yields, on the mutual orientation of their transition dipole moments, as expressed by the geometric orientation factor, κ^2, as well as on their dynamics.[43−45] As demonstrated previously, multiparameter single-molecule FRET analysis can contribute to separate these different contributions to the observed transfer efficiency.[46] In view of our experimental results, both the observed heterogeneity in fluorescence quantum yield and in the orientation of the dye label have to be taken into account for the accurate interpretation of FRET experiments on DNA helices.[6,12] In the almost universally applied dynamic averaging regime of FRET moieties, where $\langle\kappa^2\rangle = {}^2/_3$, the usual approximation that both the donor and acceptor transition moments sample all orientations with equal probability during the transfer time is made.[43] Having established the exact restrains for the orientation and dynamics for one of the two FRET dyes commonly used in nucleic acid research,[8,19,21] e.g., the acceptor molecule terminally attached to the DNA duplex in a similar manner as that observed for Rhodamine 6G, we have reduced the problem of accurate κ^2-values to the determination of the actual orientation and dynamics of the complementary fluoro-

(43) Förster, T. *Z. Naturforsch.* **1949**, *4a*, 321−327.
(44) Stryer, L. *Annu. Rev. Biochem.* **1978**, *47*, 819−846.
(45) Dale, R. E.; Eisinger, J.; Blumberg, W. E. *Biophys. J.* **1979**, *26*, 161−194.
(46) Rothwell, P. J.; Berger, S.; Kensch, O.; Felekyan, S.; Antonik, M.; Wöhrl, B. M.; Restle, T.; Goody, R. S.; Seidel, C. A. M. *Proc. Natl. Acad. Sci. U.S.A.* **2003**, *100*, 1655−1660.

phore, e.g., of a hypothetical donor fluorophore covalently attached to the DNA helix. Note that the assignment of FRET dyes to the donor and acceptor is arbitrary, since the dipole−dipole interaction is symmetric in the sense of interchanging their positions. For illustration purposes, we will discuss in the following two representative cases of the orientational dynamics of a hypothetical donor in the context of the static acceptor with a transition moment oriented perpendicular to the helix axis, as was found in this study:

Case (i): For a completely random dynamic orientation of the donor moiety, which is a good approximation for a fluorescein dye attached to dsDNA helix via a flexible linker,[18,21] and a fixed orientation of Rh6G as an acceptor dye as described in this paper, $\langle\kappa^2\rangle$ is known to reduce from $^2/_3$[45] to $^1/_3$.[44,45] Consequently, the derived FRET distance would be 12% smaller than that for the case where both donor and acceptor positions are dynamically and completely randomly averaged. Despite the conformational heterogeneity of the stacked acceptor moiety, a unique static conformation of the acceptor can be assumed on the nanosecond time scale of FRET, which is orders of magnitude faster than the observed millisecond exchange dynamics between conformers.

Case (ii): In the case where not only the acceptor but also the hypothetical donor moiety exhibits a quasi-static orientation and slow dynamics similar to the one observed for Rhodamine 6G, the effects of both the mutual orientation and separation distance between donor and acceptor moieties on the FRET efficiency cannot be separated without prior additional knowledge of the donor's structure and dynamics. In the absence of structural heterogeneity, such orientational control of FRET has recently been demonstrated by Lewis et al.,[47] where the helical scaffold of DNA with chemically fixated donor−acceptor orientations was used. If, however, the orientational heterogeneity of one or both FRET moieties cannot be ignored, as observed for commonly used rhodamine and cyanine dyes attached to the DNA via a flexible linker, the picture becomes more complex: Each quasi-static mutual orientation of donor and acceptor transition dipole moments associated to each combination of acceptor and donor conformations yields a distinct value of the orientation factor, which in general can vary from 0 to 4. Consequently, the measured ensemble-averaged FRET efficiency is the weighted sum of the transfer efficiencies for each combination of distinct acceptor and donor conformations where the weights are given by their relative populations. In single-molecule FRET studies where transfer efficiencies are monitored and analyzed in real time, particular care must be taken when FRET efficiencies are transformed into conformational changes of the DNA structure of interest: A slow transition between distinct mutual orientations cannot be distinguished from changes of the donor−acceptor separation distance often occurring on a similar time scale of milliseconds.

(47) Lewis, F. D.; Zhang, L.; Zuo, X. *J. Am. Chem. Soc.* **2005**, *127*, 10002−10003.

Conclusion

As demonstrated in this work for a single rhodamine dye terminally attached to a DNA duplex, the determination of the orientational and dynamical heterogeneity of both the FRET donor and the acceptor moieties by means of single-molecule fluorescence in combination with NMR spectroscopy has the potential to allow for the transformation of measured FRET efficiencies into exact restrains for long-range intramolecular distances. This provides valuable structure information in biomolecular research that is complementary to NMR studies.

Acknowledgment. This work was supported by the Max-Planck Society, the Deutsche Forschungsgemeinschaft, the Fonds der Chemischen Industrie, and the Volkswagen-Stiftung. We thank Bernhard H. Geierstanger, Jochen Junker, Stefan Diekmann, Timo Fleig, and Christel Marian for fruitful discussions. C.A.M.S. gratefully acknowledges financial support by the BMBF Biofuture Grant 0311865, the SFB 663, and the Heinrich-Heine-Universität. C.G. and J.T. thank the European Commision (No. NMP4-CT-2003-505669, CIDNA) for support. A.V. acknowledges funding via a Max-Planck Research Fellowship and by the Boehringer Ingelheim Fund.

Supporting Information Available: Details on experimental methods used for the determination of exchange rates for Rhodamine-6G protons from NOESY spectra, for the analysis of single-molecule fluorescence, FCS, and sub-ensemble spectroscopy data; Results for a set of additional ds-oligonucleotide sequences studied by single-molecule MFD and FCS spectroscopy, and the complete set of figures and tables containing the NMR spectra and chemical shift values. Coordinates of the identified NMR structures of Rh6G-dsDNA have been deposited with the Protein Data Bank, entry code **2v3l**. This material is available free of charge via the Internet at http://pubs.acs.org.

JA0722574